

# Distinguishing Majorana bound states from localized Andreev bound states by interferometry

Michael Hell,<sup>1,2</sup> Karsten Flensberg,<sup>1</sup> and Martin Leijnse<sup>1,2</sup>

<sup>1</sup>*Center for Quantum Devices and Station Q Copenhagen, Niels Bohr Institute, University of Copenhagen, DK-2100 Copenhagen, Denmark*

<sup>2</sup>*Division of Solid State Physics and NanoLund, Lund University, Box. 118, S-22100, Lund, Sweden*

(Dated: January 31, 2018)

Experimental evidence for Majorana bound states (MBSs) is so far mainly based on the robustness of a zero-bias conductance peak. However, similar features can also arise due to Andreev bound states (ABSs) localized at the end of an island. We show that these two scenarios can be distinguished by an interferometry experiment based on embedding a Coulomb-blockaded island into an Aharonov-Bohm ring. For two ABSs, when the ground state is nearly degenerate, cotunneling can change the state of the island and interference is suppressed. By contrast, for two MBSs the ground state is nondegenerate and cotunneling has to preserve the island state, which leads to  $h/e$ -periodic conductance oscillations with magnetic flux. Such interference setups can be realized with semiconducting nanowires or two-dimensional electron gases with proximity-induced superconductivity and may also be a useful spectroscopic tool for parity-flip mechanisms.

PACS numbers: 71.10.Pm, 74.50.+r, 74.78.-w

Andreev bound states (ABSs) are coupled particle-hole excitations of superconductors bound to impurities [1–3], to their surface [4], or in junctions [5] with an energy in the superconducting gap. Since an ABS is a fermionic excitation, its field operator  $f = \gamma_1 + i\gamma_2$  can be decomposed into a pair of Majorana operators  $\gamma_1 = \gamma_1^\dagger, \gamma_2 = \gamma_2^\dagger$ . While the corresponding wave functions overlap in space in most cases, they can also be spatially separated for topological superconductors with triplet pairing [6–10]. This pins the energy of these Majorana bound states (MBSs) robustly to the middle of the superconducting gap and renders their non-Abelian exchange statistics accessible through braiding [11–21]. Both properties may be useful for quantum computation [22–24].

Topological superconductors may be realized in semiconductors with strong spin-orbit coupling, proximity-induced superconductivity, and magnetic fields [25, 26]. Evidence for MBSs in these systems is based on a robust zero-bias conductance peak [27–36] as predicted by theory [37–41]. However, such a peak can also be caused by disorder [42], multi-band effects [43], weak antilocalization [44], the Kondo effect [45] and, in particular, ABSs [46, 47]. To rule out disorder effects, intensive efforts have been made to fabricate cleaner devices [48–52].

Distinguishing MBSs from ABSs is one of the most urgent goals in Majorana research. What we refer to here as ABSs are modes with a large Majorana overlap. If ABSs are extended along the island, they may be discriminated from MBSs by probing a finite conductance in the middle of the island or by a strong response to a gate affecting the middle region. However, one cannot discriminate ABSs from MBSs in this way if there are two terminal ABSs, i.e., one ABS localized at each end of an

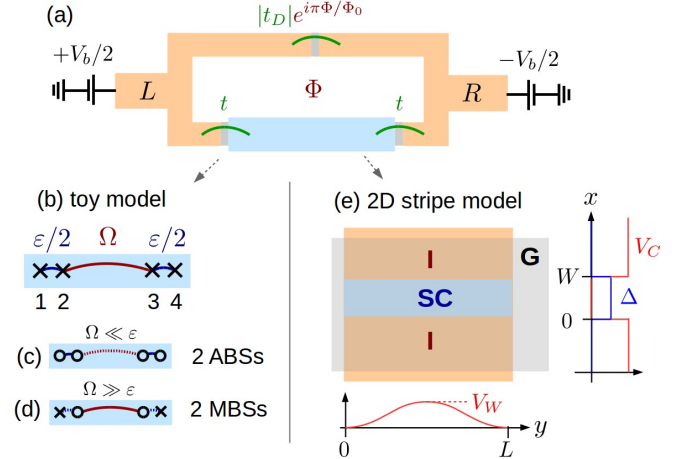


FIG. 1: Sketch of interferometer model. (a) Two normal conducting leads (orange, labeled  $L$  and  $R$ ) are connected via a superconducting island (blue) and a reference arm. (b) Toy model for the island consisting of four Majoranas, tunable from (c) two terminal ABSs to (d) two terminal MBSs. (e) 2D model for a Majorana stripe as seen from top: A stripe of superconductor (SC, blue) is placed on top of a semiconductor (orange) and induces a superconducting gap (blue in side graph). A gate on top (G, gray) induces a transverse confinement potential  $V_C$  (red in side graph). Increasing a potential barrier  $V_W$  (red in bottom graph) along the stripe tunes the stripe from case (d) to (c). Majoranas that are weakly (strongly) coupled to others are depicted by circles with a connecting line.

island [Fig. 1(c)]. While the general expectation is that ABSs do not show a similar robustness against parameter variations as MBSs, ABSs can stick close to zero energy under special conditions when the longitudinal confinement potential is smooth [53, 54]. This situation has to

be contrasted with the desired situation of two MBSs [Fig. 1(d)] when the potential is rather uniform and rises sharply at the end of the island.

In this Rapid Communication, we show how to distinguish the case of two terminal ABSs close to zero energy from the case of two terminal MBSs by embedding a Coulomb-blockaded island into an interferometric setup [Fig. 1(a)]. Interferometers have been proposed earlier to detect MBSs in grounded [55–61] and floating [62–66] devices and also to distinguish MBSs from ABSs [60, 64]. The advantages of our proposal are that it (i) relies on a standard charge current measurement, (ii) successfully distinguishes between MBSs and ABSs also when the MBSs are not fully localized, and (iii) can straightforwardly be implemented using current fabrication capabilities.

We focus on the case when the charging energy  $E_C$  is the dominant energy scale (besides the superconducting gap  $\Delta$ ) as in Majorana box qubits [67, 68]. This allows us to study the transport in the cotunneling regime when the total charge on the island is fixed. This also fixes the total fermion parity of the ground state, which can be (almost) two-fold degenerate in the case of two ABSs, while it is nondegenerate for two MBSs. Thus, cotunneling processes cannot change the state of the island for two MBSs and allow for a large interference contrast. This is different from the limiting case of two localized ABSs, in which the parity of both ABSs can be flipped [64]. This conserves the total fermion parity and reduces the interference contrast strongly. We show that this mechanism, captured by a toy model [Fig. 1(b)], also holds when using a microscopic 2D model of the island [Fig. 1(e)] tuning between the two limits.

*Toy model.* Let us consider an island that hosts four Majoranas 1, . . . 4, two localized at each end [Fig. 1(b)]. The Hamiltonian reads

$$H_I = i\varepsilon(\gamma_1\gamma_2 + \gamma_3\gamma_4) - i\Omega\gamma_2\gamma_3 + E_{C,n}, \quad (1)$$

where we included the charging energy of the island  $E_{C,n} = E_C(n - n_g)^2$ . Here,  $n$  is the number operator for the electrons on the island and  $n_g$  describes the gating. The above toy model interpolates between the situation of two terminal ABSs and two terminal MBSs: When  $\Omega \ll \varepsilon$ , two ABS are at energy  $\approx \varepsilon$  [Fig. 1(c)]. As they are formed predominantly by the Majorana operators  $(\gamma_1, \gamma_2)$  and  $(\gamma_3, \gamma_4)$ , we will denote them by  $\langle 12 \rangle$  and  $\langle 34 \rangle$ , respectively. By contrast, when  $\Omega \gg \varepsilon$ , there are two terminal MBSs [Fig. 1(d)]. The corresponding Majorana operators  $(\gamma_1, \gamma_4)$  form a mode  $\langle 14 \rangle$  with a small energy  $\approx \varepsilon^2/2\Omega$ . In addition, the pair of Majorana operators  $(\gamma_2, \gamma_3)$  forms a mode  $\langle 23 \rangle$  at higher energy  $\approx 2\Omega$ .

*Interferometer model.* The interferometer is enclosed between two nonsuperconducting leads described by  $H_0 = \sum_{rk\sigma} (\varepsilon_{rk} - \mu_r) c_{rk\sigma}^\dagger c_{rk\sigma}$ , where  $c_{rk\sigma}$  denotes the annihilator for electrons in lead  $r = L, R$  in mode  $k$  with spin  $\sigma = \uparrow, \downarrow$ . The leads are held at a common

temperature  $T$  and are voltage-biased symmetrically:  $\mu_L = -\mu_R = V_b/2$  (We set  $e = \hbar = c = k_B = 1$ ).

The tunnel Hamiltonian reads

$$H_T = \sum_{rk\sigma m=1,2} c_{rk\sigma} e^{i\varphi/2} t_{r\sigma m} (\delta_{rL} \gamma_m + \delta_{rR} \gamma_{5-m}) + \sum_{kk'\sigma\sigma'} t_{D,\sigma\sigma'} c_{Lk\sigma}^\dagger c_{Rk'\sigma'} + \text{H.c.}, \quad (2)$$

where  $\varphi$  denotes the superconducting phase on the island and  $m = 1, 2$  enumerates the Majorana operators. In our toy model, we assume that lead  $r$  couples only to the two nearest MBSs [first line of Eq. (2)] with energy-independent tunnel matrix elements  $t_{r\sigma m}$ . For simplicity, we assume the island to be left-right symmetric, so that they obey the relation  $t_{L\sigma m} = (-1)^m \sigma t_{R\bar{\sigma}m} = t_{\sigma m}$  [69]. By rotating the spin basis in the leads, one can parametrize the tunnel matrix elements conveniently as  $t_{\uparrow 1} = t \cos(\lambda)$ ,  $t_{\downarrow 1} = 0$ ,  $t_{\uparrow 2} = t \sin(\lambda) \cos(\beta) e^{i\delta}$ , and  $t_{\downarrow 2} = t \sin(\lambda) \sin(\beta) e^{i\delta}$  [69]. The parameter  $t$ , together with the spin- and energy-independent density of states  $\nu$  of the leads sets the overall tunnel rate  $\Gamma = 2\pi\nu|t|^2$  between the leads and the island,  $\lambda$  characterizes the relative coupling strength of the two Majoranas to the leads,  $\delta$  is a relative phase shift, and  $\beta$  is the canting of the different spin directions the two Majoranas couple to.

In our model, a featureless reference arm connects the two leads [second term in Eq. (2)]. The phase of the direct tunnel amplitude  $t_{D,\sigma\sigma'} = |t_D|(\delta_{\sigma\sigma'} + \tau_{\text{sf}}\delta_{\sigma\bar{\sigma}'})e^{i\pi\Phi/\Phi_0}$  is controlled by the magnetic flux  $\Phi$  threaded through the loop ( $\Phi_0 = e/2h$ ). We neglect here decoherence in the reference arm, which is motivated by the experimental observation of phase-coherent transport up to several  $\mu\text{m}$  in InAs [51, 70] and InGaAs [71] interferometers. Note that if  $\lambda = 0$  or  $\beta = 0$ , the island couples only to electrons with spin  $\uparrow$  ( $\downarrow$ ) in the left (right) lead. In the special case when the tunneling in the reference arm is spin-conserving ( $\tau_{\text{sf}} = 0$ ), no interference can appear because one can tell from the spin of the outgoing electron which path has been taken [72]. In practice, the island is of course not perfectly symmetric and spin-orbit coupling rotates the spin of electrons traveling through the reference arm, resulting in a nonzero interference. For simplicity, we set  $\tau_{\text{sf}} = 1$ , which limits the interference contrast to 1/2 when  $\beta = 0$  [Eq. (4)].

*Transport calculations.* Our goal is to understand the behavior of the maximal interference contrast:

$$\text{MIC} := \max_{\Phi, |t_D|} \left| \frac{I(\Phi) - I(\Phi + \Phi_0)}{I(\Phi) + I(\Phi + \Phi_0)} \right|. \quad (3)$$

Here,  $I(\Phi)$  is the stationary current through the interferometer. Note that the maximal or minimal current may not necessarily flow for  $\Phi = 0, \pi$ . Since interference requires coherent transport through the island, we constrain our calculations to the cotunneling regime. We set up a master equation [69] and consider the specific

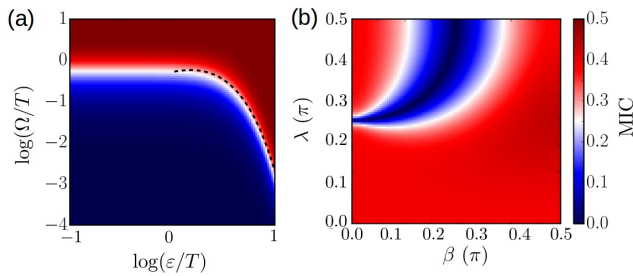


FIG. 2: Parameter dependence of the MIC for the toy model. (a) Dependence on Majorana coupling energies for  $\lambda = \beta = 0$ . The black-dashed line is given by  $\Omega = \sqrt{2\varepsilon^3/T}e^{-\varepsilon/T}$  and marks the crossover between transport dominated by parity-conserving and parity-flipping cotunneling. (b) Dependence on tunnel matrix elements for  $\Omega/T = 1$ ,  $\varepsilon/T = 0.1$ . In both cases, we used  $V_b = 0.01T$ ,  $U = 100T$ , and  $\delta = 0$ .

situation when only one particular charge state  $n = n_0$  of the island is occupied and cotunneling predominantly involves only the adjacent charge state  $n_0 + 1$  ( $\Gamma, T, V_b \ll U = E_{C,n_0+1} - E_{C,n_0} \ll E_{C,n_0} - E_{C,n_0-1}$ ). Without loss of generality, we assume  $n_0$  to be even. While our toy model neglects cotunneling through the quasiparticle continuum, quasiparticle states are included partially later on in the 2D island model. The cotunneling rates are computed with the T-matrix approach including terms of  $O(t^2, t_D)$  into the T-matrix [69]. We neglect all other contributions, including those leading to the Kondo effect ( $\Gamma, T_K \ll T$ ) and Cooper-pair cotunneling forming a virtual intermediate Cooper pair ( $\Gamma \ll U, \Delta$ ).

*Interference contrast for toy model.* To contrast the cases of two MBSs and two ABSs, we first study the parameter dependence of the MIC for the toy model (5). When  $\beta = \delta = 0$  and  $V_b \ll E = \sqrt{\varepsilon^2 + \Omega^2} \ll U$ , the MIC reads

$$\text{MIC} = \frac{\tanh(E/T)}{2\sqrt{1 + \left(\frac{E/\Omega}{\cos^2(2\lambda)} - 1\right) \frac{2E/T}{\sinh(2E/T)}}}. \quad (4)$$

Details including an expression for general bias voltage are given in [69]. We see that the MIC tends to its maximal value when  $\Omega/\varepsilon \gg 1$  (two MBSs), while it tends to zero when  $\Omega/\varepsilon \ll 1$  (two ABSs) [Fig. 2(a)]. This implies that the case of two MBSs and two ABSs can be distinguished by the maximally achievable MIC. In the next two paragraphs, we explain the different behavior of the two cases when only Majoranas 1 and 4 are connected to the leads ( $\lambda = 0$ ).

When  $\Omega/\varepsilon \gg 1$  and  $\Omega \gg V_b, T$ , the island resides mostly in its ground state, in which the parities of the modes  $\langle 23 \rangle$  and  $\langle 14 \rangle$  are even. Transport is predominantly carried by parity-conserving cotunneling processes: An electron incoming from one lead flips the parity of mode  $\langle 14 \rangle$  and the outgoing electron flips it back. Such electrons interfere with electrons tunneling through

the reference arm and lead to a large MIC [Fig. 2(a)]. The MIC is suppressed when voltage bias or temperature exceed the inelastic cotunneling threshold, i.e., when  $\min(V_b, T) > E$  [Fig. 2(a)]. In this case cotunneling processes can flip the parity of the modes  $\langle 14 \rangle$  and  $\langle 23 \rangle$  and bring the island from its ground state to the excited state. We will refer to this as parity-flipping processes (referring to the individual modes) even though the total fermion parity of the island is of course preserved. The occupation probability of the ground and excited state tend to  $1/2$  when  $\min(V_b, T) \gg E$ . Importantly, the flux dependence of the cotunneling rates differs by  $\pi$  depending on the initial parity of mode  $\langle 23 \rangle$  in the cotunneling process [62]. Hence, interference is still possible in each cotunneling event but the MIC becomes suppressed due to averaging over both possible initial states.

When  $\Omega/\varepsilon \ll 1$ , the MIC can be suppressed even if  $E \gg \max(V_b, T)$ . The reason is that parity-conserving cotunneling is strictly forbidden in the limit  $\Omega = 0$ : The left lead couples only to mode  $\langle 12 \rangle$ , while the right lead only couples to mode  $\langle 34 \rangle$ . A cotunneling process transferring an electron from one to another must therefore flip the parities of both modes and thus results in the final state being different from the initial state. Hence, there is no interference. When  $\varepsilon > T$ , the crossover from transport dominated by parity-conserving to parity-flipping processes happens when  $\Omega > \sqrt{2\varepsilon^3/T}e^{-\varepsilon/T}$  ( $V_b \ll T$ ) [Fig. 2(a)]. In experiments, this crossover may be influenced by other processes that can flip the parities of the ABSs, such as quasiparticle poisoning from the continuum [73], or Cooper-pair splitting due to photons [74] or phonons [75]. If the current is averaged over a time shorter than the time between two parity flips, interference remains detectable and the parity of mode  $\langle 23 \rangle$  can be read out [67]. The MIC may thus also be utilized to measure such rates. The results we show here have to be understood as long-time averages of many parity flips instead.

The qualitative parameter dependence of the MIC remains in most cases unchanged if one considers the general case of  $\lambda \neq 0, \beta \neq 0, \delta \neq 0$ . From numerical calculations, we find only a weak dependence of the MIC on  $\delta$  except for special points [69]. We find, however, a suppression of the MIC under the condition  $\sqrt{(\lambda - \pi/2)^2 + \beta^2} \approx \pi/4$  [Fig. 2(b) and Eq. (4)]. Here, the parity-conserving cotunneling rates vanish because of destructive interference of processes involving only the island (not the reference arm). We finally note that the case  $\Omega = 0$  with  $\varepsilon = 0$  or  $\lambda = 0$  is a pathological case of our model [69].

*2D model for Majorana stripe.* To see whether the simple toy model discussed so far indeed captures the main physics to contrast the cases of two MBSs and two ABSs, we next turn to a more sophisticated model for the island. Following [76], we consider a Majorana stripe of width  $W$  and length  $L$  defined in a two-dimensional

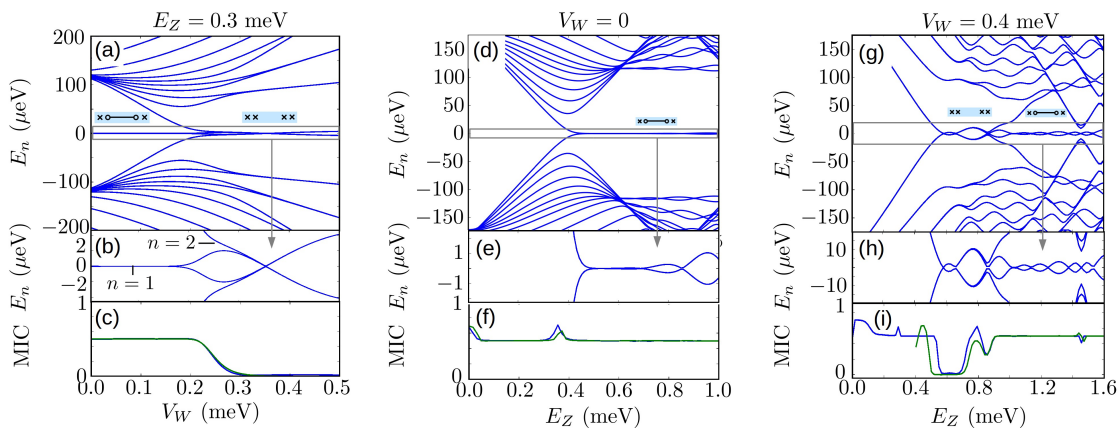


FIG. 3: Suppression of the interference contrast for the transition from two MBSs to two ABSs. We show the energy spectrum of the stripe Hamiltonian (5) (upper panels) with close-ups around zero energy (middle panels) alongside the MIC (lower panels). We compute the MIC both for the 2D stripe model (blue) and the toy model with parameters extracted from the 2D stripe model (green) [69]. The values of  $E_Z$  and  $V_W$  are specified in the panels, the lattice constant is  $a = 10$  nm,  $\Delta = 180$   $\mu$ eV,  $E_{\text{SO}} = m^* \alpha^2 / 2 = 116.5$   $\mu$ eV,  $\mu = 0$ ,  $V_C = 1$  meV,  $W = 200$  nm,  $L = 2$   $\mu$ m,  $m^* = 0.023 m_e$ ,  $U = 50$   $\mu$ eV,  $T = 1.6$   $\mu$ eV ( $\approx 20$  mK), and  $V_b = 1$   $\mu$ eV. In (i), the toy model breaks down for  $E_Z \lesssim 0.4$  meV (see text).

electron gas [Fig. 1(e)]. The electron gas is modeled by a single electron band with effective mass  $m^*$  at chemical potential  $\mu$  as described by the following Bogoliubov-de Gennes Hamiltonian:

$$\mathcal{H}_{\text{BdG}} = \left( -\frac{\partial_x^2 + \partial_y^2}{2m^*} + V_C(x) + V_W(y) - \mu \right) \tau_z \quad (5)$$

$$-i\alpha(\sigma_x \partial_y - \sigma_y \partial_x) \tau_z + E_Z \sigma_y / 2 + \Delta(x) \tau_x.$$

In the second line, we added the Rashba spin-orbit coupling (with velocity  $\alpha$ ), the Zeeman energy ( $E_Z$ ) due to a magnetic field, and the induced superconducting gap. The latter is nonzero where the electron gas is covered by the superconductor:  $\Delta(x) = \Delta \Theta(W/2 - |x|)$ . The Hamiltonian acts on the four-component spinor  $[u_\uparrow(x, y), u_\downarrow(x, y), v_\downarrow(x, y), -v_\uparrow(x, y)]^T$  containing the electron ( $u$ ) and hole ( $v$ ) components for spin  $\sigma = \uparrow, \downarrow$ . The Pauli matrices  $\tau_i$  and  $\sigma_i$  ( $i = x, y, z$ ) act on particle-hole and spin space, respectively. Gates are used to confine the states in the transverse direction,  $V_C(x) = V_C \Theta(|x| - W/2)$  ( $V_C \gg \mu, \Delta, E_Z, E_{\text{SO}} = m\alpha^2/2$ ). Equation (5) also models a nanowire if the transverse confinement in one direction is much stronger than in the other (e.g. due to gating) [77–79].

*Tuning from two MBSs to two ABSs.* Accounting for an additional potential profile along the stripe,  $V_W(y) = V_W[1 + \cos(2\pi y/L)]$ , we can tune from the case of two MBSs to two ABSs by increasing  $V_W$ . Computing the energy spectrum of the island [Fig. 3(a)], we find for  $V_W = 0$  only one mode ( $n = 1$ ) close to zero energy. This mode is formed by two slightly overlapping MBSs at opposite ends of the stripe. When increasing  $V_W$ , the second mode ( $n = 2$ ) comes close to and sticks to zero energy [Fig. 3(b)]. When  $V_W$  is large, the two modes correspond to two ABSs localized at the ends of the wire

[69]. The MIC is reduced when  $V_W$  is increased as the system evolves from two MBSs to two ABSs [Fig. 3(c)].

To compute the MIC using the 2D model, we include the 8 lowest modes into our master equation approach. We further extracted the parameters for the toy model (yielding the tunnel matrix elements) of the two lowest modes obtained for the 2D model. In this extraction procedure [69], we neglect the coupling of the Majoranas on the left (right) to the right (left) lead. We find that the toy model reproduces the MIC rather accurately.

We finally discuss the magnetic-field dependence of the MIC [Figs. 3(d)–(i)]. Similar to the case of two MBSs, the energies of the two ABSs oscillate around zero energy as a function of magnetic field [compare Figs. 3(e) and (h)]. For  $V_W = 0$ , we see that the MIC also stays large in the nontopological regime for small values of  $E_Z$  [Fig. 3(f)]. The reason is that parity-flipping processes are energetically forbidden as long as  $2(E_1 + E_2) \ll V_b, T$ . However, when  $E_Z$  is small, the Coulomb peaks are not  $1e$  periodic [33], which is a way to distinguish the non-topological from the topological regime in this case.

For the case of two ABSs ( $V_W = 0.4$  meV), we find that the MIC is suppressed when there are two modes close to zero energy [Fig. 3(i)]. The MIC is restored again when at least one of the modes has an energy  $\gg V_b, T$ . This happens for small magnetic fields [ $E_Z < 0.5$  meV in Fig. 3(i)] when the ABSs are at large energies or when the case of two MBSs is restored [ $E_Z > 0.9$  meV in Fig. 3(i)]. Again, for small  $E_Z$ , the Coulomb peaks are not  $1e$  periodic, which rules out the presence of MBSs. We note that the toy model breaks down in this regime because  $\Omega/\varepsilon$  becomes very small (leading to nearly zero current through the island). This does not happen for the full

2D model where all tunnel couplings are accounted for.

*Conclusion.* A zero-bias conductance peak in transport spectroscopy of superconducting islands can arise due to MBSs as well as ABSs. While extended ABSs may be probed by a contact in the middle of a superconducting stripe, terminal ABSs cannot. We have shown that terminal ABSs can instead be distinguished from two terminal MBSs by an interference experiment. Such experiments may also be useful to probe quasiparticle-poisoning rates for nonisolated islands. Finally, the idea of our approach may be of interest for initial testing of the presence of MBS in Majorana-qubit devices [21, 67], in which interferometers are integrated as a means of readout.

We acknowledge stimulating discussions with M. Deng, A. Fornieri, L. Glazman, C. M. Marcus, F. Nichele, E. O'Farrell, S. Plugge, A. Stern, A. Whiticar, and support from the Crafoord Foundation (M. L. and M. H.), the Swedish Research Council (M. L.), The Danish National Research Foundation, and from the Microsoft Station Q Program.

- 
- [1] L. Yu, *Acta Physica Sinica* **21**, 75 (1965).  
 [2] H. Shiba, *Progress of Theoretical Physics* **40**, 435 (1968).  
 [3] A. Rusinov, *Soviet Journal of Experimental and Theoretical Physics Letters* **9**, 85 (1969).  
 [4] T. Löfwander, V. Shumeiko, and G. Wendin, *Superconductor Science and Technology* **14**, R53 (2001).  
 [5] I. Kulik, *Soviet Journal of Experimental and Theoretical Physics* **30**, 944 (1969).  
 [6] A. Y. Kitaev, *Sov. Phys.–Uspeki* **44**, 131 (2001).  
 [7] J. Alicea, *Rep. Prog. Phys.* **75**, 076501 (2012).  
 [8] M. Leijnse and K. Flensberg, *Semicond. Sci. Technol.* **27**, 124003 (2012).  
 [9] C. W. J. Beenakker, *Annu. Rev. Con. Mat. Phys.* **4**, 113 (2013).  
 [10] T. D. Stanescu and S. Tewari, *J. Phys.: Condens. Matter* **25**, 233201 (2013).  
 [11] J. Alicea, Y. Oreg, G. Refael, F. von Oppen, and M. P. A. Fisher, *Nat. Phys.* **7**, 412 (2011).  
 [12] D. J. Clarke, J. D. Sau, and S. Tewari, *Phys. Rev. B* **84**, 035120 (2011).  
 [13] B. I. Halperin, Y. Oreg, A. Stern, G. Refael, J. Alicea, and F. von Oppen, *Phys. Rev. B* **85**, 144501 (2012).  
 [14] T. Hyart, B. van Heck, I. C. Fulga, M. Burrello, A. R. Akhmerov, and C. W. J. Beenakker, *Phys. Rev. B* **88**, 035121 (2013).  
 [15] D. Aasen, M. Hell, R. V. Mishmash, A. Higginbotham, J. Danon, M. Leijnse, T. S. Jespersen, J. A. Folk, C. M. Marcus, K. Flensberg, et al., *Phys. Rev. X* **6**, 031016 (2016).  
 [16] M. Hell, J. Danon, K. Flensberg, and M. Leijnse, *Phys. Rev. B* **94**, 035424 (2016).  
 [17] J. D. Sau, D. J. Clarke, and S. Tewari, *Phys. Rev. B* **84**, 094505 (2011).  
 [18] B. van Heck, A. R. Akhmerov, F. Hassler, M. Burrello, and C. W. J. Beenakker, *New Journal of Physics* **14**, 035019 (2012).  
 [19] P. Bonderson, *Phys. Rev. B* **87**, 035113 (2013).  
 [20] S. Vijay and L. Fu, *Phys. Rev. B* **94**, 235446 (2016).  
 [21] T. Karzig, C. Knapp, R. M. Lutchyn, P. Bonderson, M. B. Hastings, C. Nayak, J. Alicea, K. Flensberg, S. Plugge, Y. Oreg, et al., *Phys. Rev. B* **95**, 235305 (2017).  
 [22] S. Bravyi and A. Kitaev, *Annals of Physics* **298**, 210 (2002).  
 [23] S. Bravyi and A. Kitaev, *Phys. Rev. A* **71**, 022316 (2005).  
 [24] M. H. Freedman, A. Kitaev, M. J. Larsen, and Z. Wang, *Bull. Amer. Math. Soc.* **40**, 31 (2003).  
 [25] Y. Oreg, G. Refael, and F. von Oppen, *Phys. Rev. Lett.* **105**, 177002 (2010).  
 [26] R. M. Lutchyn, J. D. Sau, and S. Das Sarma, *Phys. Rev. Lett.* **105**, 077001 (2010).  
 [27] V. Mourik, K. Zuo, S. M. Frolov, S. R. Plissard, E. P. A. M. Bakkers, and L. P. Kouwenhoven, *Science* **336**, 1003 (2012).  
 [28] A. Das, Y. Ronen, Y. Most, Y. Oreg, M. Heiblum, and H. Shtrikman, *Nat. Phys.* **8**, 887 (2012).  
 [29] A. D. K. Finck, D. J. Van Harlingen, P. K. Mohseni, K. Jung, and X. Li, *Phys. Rev. Lett.* **110**, 126406 (2013).  
 [30] L. P. Rokhinson, X. Liu, and J. K. Furdyna, *Nat. Phys.* **8**, 795 (2012).  
 [31] M. T. Deng, C. L. Yu, G. Y. Huang, M. Larsson, P. Caroff, and H. Q. Xu, *Nano Lett.* **12**, 6414 (2012).  
 [32] H. O. H. Churchill, V. Fatemi, K. Grove-Rasmussen, M. T. Deng, P. Caroff, H. Q. Xu, and C. M. Marcus, *Phys. Rev. B* **87**, 241401 (2013).  
 [33] S. M. Albrecht, A. P. Higginbotham, M. Madsen, F. Kuemmeth, T. S. Jespersen, J. Nyg, P. Krogstrup, and C. M. Marcus, *Nature* **531**, 206 (2016).  
 [34] M. Deng, S. Vaitiekėnas, E. B. Hansen, J. Danon, M. Leijnse, K. Flensberg, J. Nygård, P. Krogstrup, and C. M. Marcus, *Science* **354**, 1557 (2016).  
 [35] H. J. Suominen, M. Kjaergaard, A. R. Hamilton, J. Shabani, C. J. Palmström, C. M. Marcus, and F. Nichele, *arXiv preprint arXiv:1703.03699v1* (2017).  
 [36] F. Nichele, A. C. Drachmann, A. M. Whiticar, E. C. O'Farrell, H. J. Suominen, A. Fornieri, T. Wang, G. C. Gardner, C. Thomas, A. T. Hatke, et al., *Phys. Rev. Lett.* **119**, 136803 (2017).  
 [37] C. J. Bolech and E. Demler, *Phys. Rev. Lett.* **98**, 237002 (2007).  
 [38] K. T. Law, P. A. Lee, and T. K. Ng, *Phys. Rev. Lett.* **103**, 237001 (2009).  
 [39] K. Flensberg, *Phys. Rev. B* **82**, 180516 (2010).  
 [40] A. Golub and B. Horovitz, *Phys. Rev. B* **83**, 153415 (2011).  
 [41] M. Wimmer, A. R. Akhmerov, J. P. Dahlhaus, and C. W. J. Beenakker, *New J. Phys.* **13**, 053016 (2011).  
 [42] D. Bagrets and A. Altland, *Phys. Rev. Lett.* **109**, 227005 (2012).  
 [43] J. Liu, A. C. Potter, K. T. Law, and P. A. Lee, *Phys. Rev. Lett.* **109**, 267002 (2012).  
 [44] D. I. Pikulin, J. P. Dahlhaus, M. Wimmer, H. Schomerus, and C. W. J. Beenakker, *New Journal of Physics* **14**, 125011 (2012).  
 [45] D. Goldhaber-Gordon, H. Shtrikman, D. Mahalu, D. Abusch-Magder, U. Meirav, and M. Kastner, *Nature* **391** (1998).  
 [46] E. J. H. Lee, X. Jiang, R. Aguado, G. Katsaros, C. M. Lieber, and S. De Franceschi, *Phys. Rev. Lett.* **109**, 186802 (2012).

- [47] G. Kells, D. Meidan, and P. W. Brouwer, *Phys. Rev. B* **86**, 100503 (2012).
- [48] P. Krogstrup, N. L. B. Ziino, W. Chang, S. M. Albrecht, M. H. Madsen, E. Johnson, J. Nygård, C. M. Marcus, and T. S. Jespersen, *Nature Materials* **14**, 400 (2015).
- [49] W. Chang, S. M. Albrecht, T. S. Jespersen, F. Kuemmeth, P. Krogstrup, J. Nygård, and C. M. Marcus, *Nature Nanotechnology* **10**, 232 (2015).
- [50] H. Zhang, Ö. Gül, S. Conesa-Boj, M. P. Nowak, M. Wimmer, K. Zuo, V. Mourik, F. K. de Vries, J. van Veen, M. W. de Moor, et al., *Nature Communications* **8** (2017).
- [51] S. Gazibegovic, D. Car, H. Zhang, S. C. Balk, J. A. Logan, M. W. de Moor, M. C. Cassidy, R. Schmits, D. Xu, G. Wang, et al., *Nature* **548** (2017).
- [52] O. Gul, H. Zhang, F. K. de Vries, J. van Veen, K. Zuo, V. Mourik, S. Conesa-Boj, M. P. Nowak, D. J. Van Woerkerkom, M. Quintero-Pérez, et al., *Nano Letters* **17**, 2690 (2017).
- [53] G. Kells, D. Meidan, and P. W. Brouwer, *Phys. Rev. B* **86**, 100503 (2012).
- [54] C.-X. Liu, F. Setiawan, J. D. Sau, and S. Das Sarma, *Phys. Rev. B* **96**, 054520 (2017).
- [55] C. Benjamin and J. K. Pachos, *Phys. Rev. B* **81**, 085101 (2010).
- [56] S. En-Ming, P. Yi-Ming, S. Lu-Bing, and W. Bai-Gen, *Chinese Physics B* **23**, 057201 (2014).
- [57] B. Y. Sun and M. W. Wu, *New Journal of Physics* **16**, 073045 (2014).
- [58] A. Ueda and T. Yokoyama, *Phys. Rev. B* **90**, 081405 (2014).
- [59] A. Ueda and T. Yokoyama, *Physics Procedia* **58**, 182 (2014).
- [60] K. M. Tripathi, S. Das, and S. Rao, *Phys. Rev. Lett.* **116**, 166401 (2016).
- [61] D. Dahan, M. T. Ahari, G. Ortiz, B. Seradjeh, and E. Grosfeld, *Phys. Rev. B* **95**, 201114 (2017).
- [62] L. Fu, *Phys. Rev. Lett.* **104**, 056402 (2010).
- [63] A. Yamakage and M. Sato, *Physica E: Low-dimensional Systems and Nanostructures* **55**, 13 (2014).
- [64] J. D. Sau, B. Swingle, and S. Tewari, *Phys. Rev. B* **92**, 020511 (2015).
- [65] S. Rubbert and A. R. Akhmerov, *Phys. Rev. B* **94**, 115430 (2016).
- [66] C.-K. Chiu, J. D. Sau, and S. D. Sarma, arXiv preprint arXiv:1709.04475 (2017).
- [67] S. Plugge, A. Rasmussen, A. Egger, and K. Flensberg, *New Journal of Physics* **19**, 012001 (2017).
- [68] S. Plugge, L. A. Landau, E. Sela, A. Altland, K. Flensberg, and R. Egger, *Phys. Rev. B* **94**, 174514 (2016).
- [69] M. Hell, K. Flensberg, and M. Leijnse, Supplemental material to "Distinguishing Majorana bound states from localized Andreev bound states by interferometry" (2017).
- [70] C. H. Yang, M. J. Yang, K. A. Cheng, and J. C. Culbertson, *Phys. Rev. B* **66**, 115306 (2002).
- [71] S. L. Ren, J. J. Heremans, C. K. Gaspé, S. Vijayaragunathan, T. D. Mishima, and M. B. Santos, *Journal of Physics: Condensed Matter* **25**, 435301 (2013).
- [72] H. Aker, *Phys. Rev. B* **47**, 6835 (1993).
- [73] A. P. Higginbotham, S. M. Albrecht, G. Kirsanskas, W. Chang, F. Kuemmeth, P. Krogstrup, T. S. Jespersen, J. Nygard, K. Flensberg, and C. M. Marcus, *Nat. Phys.* **11**, 1017 (2015).
- [74] L. Bretheau, C. O. Girit, C. Urbina, D. Esteve, and H. Pothier, *Phys. Rev. X* **3**, 041034 (2013).
- [75] U. Patel, I. V. Pechenezhskiy, B. Plourde, M. Vavilov, and R. McDermott, arXiv preprint arXiv:1610.09351 (2016).
- [76] M. Hell, M. Leijnse, and K. Flensberg, *Phys. Rev. Lett.* **118**, 107701 (2017).
- [77] R. M. Lutchyn, T. D. Stanescu, and S. Das Sarma, *Phys. Rev. Lett.* **106**, 127001 (2011).
- [78] A. C. Potter and P. A. Lee, *Phys. Rev. Lett.* **105**, 227003 (2010).
- [79] T. D. Stanescu, R. M. Lutchyn, and S. Das Sarma, *Phys. Rev. B* **84**, 144522 (2011).

# Distinguishing Majorana bound states from localized Andreev bound states by interferometry: Supplemental Material

Michael Hell,<sup>1,2</sup> Karsten Flensberg,<sup>1</sup> and Martin Leijnse<sup>1,2</sup>

<sup>1</sup>*Center for Quantum Devices and Station Q Copenhagen, Niels Bohr Institute, University of Copenhagen, DK-2100 Copenhagen, Denmark*

<sup>2</sup>*Division of Solid State Physics and NanoLund, Lund University, Box. 118, S-22100, Lund, Sweden*

(Dated: January 31, 2018)

PACS numbers: 71.10.Pm, 74.50.+r, 68.65.La

## DETAILS OF THE MODELS

### 2D island model: Eigenmodes and energies

Since we assume that the charging energy  $E_C$  is the dominant energy scale, we work in the basis of many-body eigenstates denoted by  $|n, \boldsymbol{\eta}\rangle$ . Here,  $n$  is the number of electrons on the island and  $\boldsymbol{\eta} = (\eta_1, \eta_2, \dots)$  contains the occupations  $\eta_l$  of the eigenmodes  $l$  of the island. These modes are found by solving for the eigenstates of the BdG Hamiltonian (5):  $\mathcal{H}_{\text{BdG}}\boldsymbol{\chi}_l = \varepsilon_l\boldsymbol{\chi}_l$ . The annihilation operator for eigenmode  $l$  is given by

$$\beta_l = \int dx \int dy \boldsymbol{\chi}_l^\dagger(x, y) \cdot \boldsymbol{\psi}(x, y), \quad (\text{S1})$$

where  $\boldsymbol{\psi}(x, y) = [\psi_\uparrow(x, y), \psi_\downarrow(x, y), \psi_\downarrow^\dagger(x, y), -\psi_\uparrow^\dagger(x, y)]^T$  contains the electron field operators for spin  $\sigma = \uparrow, \downarrow$  at position  $(x, y)$ . The energies of the many-body eigenstates read

$$\varepsilon_{n, \boldsymbol{\eta}} = E_C(n - n_g)^2 + \sum_l \eta_l \varepsilon_l. \quad (\text{S2})$$

For a nonsuperconducting island, the occupations have to satisfy  $\sum_l \eta_l = n$ . This condition is lifted in the superconducting case, where they only have to obey the constraint  $(-1)^{\sum_l \eta_l} = (-1)^n$ . Since the modes  $l$  are electron-hole superpositions, the occupations  $\eta_l$  thus only specify the fermion parity  $(-1)^{\eta_l}$  of mode  $l$  but not the charge associated with occupying this mode.

### Toy model: Eigenmodes and energies

To derive the left-right symmetry relation of the Majorana tunnel couplings in Sec. , we will need the eigenstates and eigenmodes of the toy model (1). For this purpose, we first rewrite Eq. (1) as  $H_I = \frac{1}{2}\boldsymbol{\alpha}^\dagger \cdot \mathcal{H}_I \cdot \boldsymbol{\alpha}$ , where  $\boldsymbol{\alpha} = (\alpha_L, \alpha_R, \alpha_L^\dagger, \alpha_R^\dagger)^T$  contains the field operators of the modes  $\alpha_L = (\gamma_1 + i\gamma_2)/2$  and  $\alpha_R = (\gamma_3 + i\gamma_4)/2$ .

By diagonalizing the Hamiltonian matrix

$$\mathcal{H}_I = \begin{pmatrix} \varepsilon & \Omega & 0 & \Omega \\ \Omega & \varepsilon & -\Omega & 0 \\ 0 & -\Omega & -\varepsilon & -\Omega \\ \Omega & 0 & -\Omega & -\varepsilon \end{pmatrix}, \quad (\text{S3})$$

we can express the Hamiltonian as  $H_I = \frac{1}{2}\boldsymbol{\beta}^\dagger \cdot \mathcal{H}'_I \cdot \boldsymbol{\beta}$  with  $\mathcal{H}'_I = \text{diag}(\varepsilon_2, \varepsilon_1, -\varepsilon_1, -\varepsilon_2)$  and eigenenergies

$$\varepsilon_{1/2} = \sqrt{\varepsilon^2 + \Omega^2} \mp \Omega. \quad (\text{S4})$$

The field operators of the eigenmodes are again collected in a 4-component vector  $\boldsymbol{\beta} = \mathcal{U} \cdot \boldsymbol{\alpha}$ , where

$$\mathcal{U} = \begin{pmatrix} r_+ & r_+ & -r_- & r_- \\ r_+ & -r_+ & r_- & r_- \\ r_- & r_- & r_+ & -r_+ \\ -r_- & r_- & r_+ & r_+ \end{pmatrix} \quad (\text{S5})$$

and  $r_\pm = \sqrt{1 \pm 1/\sqrt{1 + (\Omega/\varepsilon)^2}}/2$ , which satisfies the relation  $r_+^2 + r_-^2 = 1/2$ .

### 2D island: Tunnel Hamiltonian

Here, we explain how to extract the tunnel matrix elements from the 4-spinor components of the solutions of the BdG equation for our transport calculations.

For the transport calculations for the 2D island model, we start from the standard bilinear tunnel Hamiltonian

$$H_T = \sum_{rk\sigma} \int dx \int dy t_r(x, y) c_{rk\sigma} e^{i\varphi/2} \psi_\sigma^\dagger(x, y) + \text{H.c.} \quad (\text{S6})$$

We use the same notation as in the main paper and introduced the field operator  $\psi_\sigma^\dagger(x, y)$  creating an electron on the island at position  $(x, y)$  with spin  $\sigma$ .

Inverting Eq. (S1) and using the particle-hole symmetry of  $\mathcal{H}_{\text{BdG}}$ ,  $[\mathcal{P}, \mathcal{H}_{\text{BdG}}]_+ = 0$  with  $\mathcal{P} = \sigma_y \tau_y \mathcal{K}$  ( $\mathcal{K}$  denotes the complex conjugation), yields

$$\psi_\sigma^\dagger(x, y) = \sum_{l \text{ unocc.}} [u_{l\sigma}^*(x, y) \beta_l^\dagger + v_{l\sigma}(x, y) \beta_l]. \quad (\text{S7})$$

The sum in Eq. (S7) includes every particle-hole conjugated mode pair only once. One is, in principle, free to choose which of the modes at energy  $\pm\varepsilon_l$  is used. The choice we use is that the sum runs only over modes  $l$  that are unoccupied at zero temperature. In the topologically trivial regime at zero magnetic field, these are all the modes with positive energy. However, when a mode crosses zero energy (such as a MBS), then the occupation of that state changes at zero temperature. When then use the mode at negative energy. We use this choice because then the correct electron-hole components will be used for the transport calculations when inserting Eq. (S7) into the tunnel Hamiltonian (S6):

$$H_T = \sum_{rk\sigma pl \text{ unocc.}} t_{rl\sigma}^p c_{rk\sigma} e^{i\varphi/2} \beta_l^p + \text{H.c.} \quad (\text{S8})$$

Here,  $p = \pm$ ,  $\beta_l^+ = \beta_l^\dagger$ ,  $\beta_l^- = \beta_l$ , where we assume a point-contact coupling of the leads so that

$$t_{L/Rl\sigma}^+ = t_{L/R}(0, \mp L/2) u_{l\sigma}^*(0, \mp L/2), \quad (\text{S9})$$

$$t_{L/Rl\sigma}^- = t_{L/R}(0, \mp L/2) v_{l\sigma}(0, \mp L/2). \quad (\text{S10})$$

In Sec. , we show how to express the tunnel amplitudes to the right lead in terms of those to the left lead [Eqs. (S13) and (S14)] provided the island exhibits a spatial inversion symmetry along the stripe direction.

For our transport calculations, we will consider only two relevant charge states  $n = 0$  and  $n = 1$  of the island. Projecting Eq. (S8) on the many-body basis  $|n, \boldsymbol{\eta}\rangle$  introduced in Sec. , we obtain

$$\tilde{H}_T = \sum_{rk\sigma\boldsymbol{\eta}_i\boldsymbol{\eta}_f} T_{r\sigma}^{\boldsymbol{\eta}_f\boldsymbol{\eta}_i} c_{rk\sigma} |1, \boldsymbol{\eta}_f\rangle \langle 0, \boldsymbol{\eta}_i| + \text{H.c.}, \quad (\text{S11})$$

with tunnel matrix elements

$$T_{r\sigma}^{\boldsymbol{\eta}_f\boldsymbol{\eta}_i} = [t_{rl\sigma}^+ \delta_{\boldsymbol{\eta}_i 0} + t_{rl\sigma}^- \delta_{\boldsymbol{\eta}_i 1}] \prod_{j \neq l} \delta_{\boldsymbol{\eta}_f, j \boldsymbol{\eta}_i, j}. \quad (\text{S12})$$

There are two contributions: The first one ( $\sim t_{rl\sigma}^+ \sim u_{l\sigma}^*$ ) describes a 'usual' tunneling process, which can also occur in a nonsuperconducting systems: An incoming electron occupies an empty mode  $l$ . The second one ( $\sim t_{rl\sigma}^- \sim v_{l\sigma}$ ) happens only in superconducting systems and describes the formation of a Cooper pair with the incoming electron, leaving the mode  $l$  empty in the final state.

## 2D model: Spatial inversion symmetry

While Eq. (S8) is generally valid for any 2D island model, we use in our calculations a 2D island Hamiltonian [Eq. (5)] that obeys a spatial inversion symmetry: It obeys  $[\mathcal{H}_{\text{BdG}}, \mathcal{V}]_- = 0$  with the unitary operator  $\mathcal{V} = \mathcal{I}_y \sigma_y$ . Here,  $\mathcal{I}_y$  is the inversion along the

stripe direction ( $y$ ) and  $\sigma_y$  is the Pauli matrix acting on spin. Thus, if  $\boldsymbol{\chi}_l$  is a solution of the BdG equation,  $\mathcal{H}_{\text{BdG}} \boldsymbol{\chi}_l = \varepsilon_l \boldsymbol{\chi}_l$ , then  $\mathcal{V} \boldsymbol{\chi}_l$  is also a solution for the BdG equation for the same energy. If the solution is nondegenerate, this implies  $\mathcal{V} \boldsymbol{\chi}_l = \xi_l \boldsymbol{\chi}_l$  with  $\xi_l = \pm 1$  because  $\mathcal{V}^2 = \mathcal{V}^\dagger \mathcal{V} = \mathbb{1}$ . The unitary transformation  $\mathcal{V}$  relates the wave-function components of an eigenstate on the left side of the island to that on the right side: Expressing  $\boldsymbol{\chi}_l = (u_{l\uparrow}, u_{l\downarrow}, v_{l\downarrow}, -v_{l\uparrow})^T$ , we obtain

$$u_{l\sigma}(x, y) = -i\xi_l \sigma u_{l\bar{\sigma}}(x, -y), \quad (\text{S13})$$

$$v_{l\sigma}(x, y) = -i\xi_l \sigma v_{l\bar{\sigma}}(x, -y). \quad (\text{S14})$$

The tunnel couplings thus satisfy the left-right symmetry

$$t_{rl\sigma}^p = ip \xi_l \sigma t_{r\bar{l}\bar{\sigma}}^p. \quad (\text{S15})$$

## Toy model: Spatial inversion symmetry

If the toy model is compatible with the 2D island model, then the tunnel couplings of the eigenstates of the toy model must also obey Eq. (S15). We next briefly explain how this translates into conditions for the Majorana tunnel couplings stated below Eq. (2) in the main paper. This symmetry of the tunnel couplings is, however, not essential to our findings, it is only convenient to reduce the number of parameters.

In terms of the localized modes  $\alpha_L^p = (\gamma_1 - ip\gamma_2)/2$  and  $\alpha_R^p = (\gamma_1 + ip\gamma_2)/2$ , the tunnel Hamiltonian can be expressed in the same form as Eq. (S8):

$$H_T = \sum_{rk} \tilde{t}_{r\sigma}^p c_{rk\sigma} e^{i\varphi/2} \alpha_r^p + \text{H.c.} \quad (\text{S16})$$

Here we use the assumption that mode  $\alpha_r$  couples only to lead  $r$ . Exploiting the transformation  $\boldsymbol{\beta} = \mathcal{U} \cdot \boldsymbol{\alpha}$  with  $\mathcal{U}$  given by Eq. (S5) and expressing the field operators according to Eq. (S1), we find the relation ( $l = 1, 2$ )

$$t_{rl\sigma}^p = (-1)^{\delta_{r,R} l} r_+ \tilde{t}_{r\sigma}^p + (-1)^{\delta_{r,L} (l-1)} r_- \tilde{t}_{r\sigma}^{p*}. \quad (\text{S17})$$

Using furthermore Eq. (S15), we obtain for  $\xi_1 + \xi_2 = 0$

$$\tilde{t}_{r\sigma}^p = -ip\sigma \xi \tilde{t}_{r\bar{\sigma}}^p \quad (\text{S18})$$

with  $\xi = (\xi_1 - \xi_2)/2 = \pm 1$ . We checked numerically that the inversion parities  $\xi_l$  of the two lowest modes are always opposite for the cases we considered (similar to the two lowest modes in a potential well). Note that the sign of  $\xi$  does not matter for the calculations of the interference contrast under the assumptions employed in this paper and we therefore set  $\xi = 1$ . Using relation (S18) and expressing  $\alpha_r^p$  in terms of Majorana operators, we arrive at Eq. (2) given in the main paper:

$$H_{T,I} = \sum_{rk\sigma m} c_{rk\sigma} e^{i\varphi/2} t_{r\sigma m} (\delta_{rL} \gamma_m + \delta_{rR} \gamma_{5-m}) + \text{H.c.} \quad (\text{S19})$$

with

$$\begin{aligned} t_{L\sigma 1} &= \frac{1}{2}(\tilde{t}_{L\sigma}^+ + \tilde{t}_{L\sigma}^-) = t_{\sigma 1}, \\ t_{L\sigma 2} &= \frac{i}{2}(\tilde{t}_{L\sigma}^+ - \tilde{t}_{L\sigma}^-) = t_{\sigma 2}, \end{aligned} \quad (\text{S20})$$

and  $t_{R\sigma m} = (-1)^m \xi \sigma t_{L\bar{\sigma}5-m}$  (a similar relation has also been established in Ref. [1] where the spin quantization is rotated).

### Parametrization of Majorana tunnel couplings

As mentioned in the main paper, the Majorana couplings can be parametrized in a simple way by applying a unitary transformation of the spin degree of freedom in the leads. Introducing  $c_{Lk\sigma} = U_{\sigma\sigma'} c'_{Lk\sigma'}$  and  $t_{\sigma m} = U_{\sigma\sigma'}^\dagger t'_{\sigma' m}$  in Eq. (S19), we obtain a tunnel Hamiltonian of the same form with  $c \rightarrow c'$  and  $t \rightarrow t'$ . Defining  $U$  in the general form

$$U = \begin{pmatrix} e^{i\kappa_\uparrow} \cos(\tau) & e^{i(-\zeta + \kappa_\uparrow)} \sin(\tau) \\ -e^{i(\zeta + \kappa_\downarrow)} \sin(\tau) & e^{i\kappa_\downarrow} \cos(\tau) \end{pmatrix}, \quad (\text{S21})$$

we can satisfy the conditions  $t'_{\uparrow 1} \in \mathbb{R}$ ,  $t'_{\downarrow 1} = 0$ ,  $\arg(t'_{\uparrow 2}) = \arg(t'_{\downarrow 2})$  by choosing

$$\tau = \arctan(|t_{\downarrow 1}/t_{\uparrow 1}|), \quad (\text{S22})$$

$$\zeta = \arg(t_{\downarrow 1}/t_{\uparrow 1}), \quad (\text{S23})$$

$$\kappa_\uparrow = -\arg(t_{\uparrow 1}), \quad (\text{S24})$$

$$\kappa_\downarrow = \kappa_\uparrow + \arg \left[ \frac{t_{\uparrow 2} + e^{-i\zeta} \tan(\tau) t_{\downarrow 2}}{t_{\downarrow 2} - e^{+i\zeta} \tan(\tau) t_{\uparrow 2}} \right]. \quad (\text{S25})$$

With this form of the Majorana couplings  $t'_{\sigma m}$ , they can be parametrized as

$$t'_{\uparrow 1} = t \cos(\lambda), \quad (\text{S26})$$

$$t'_{\downarrow 1} = 0, \quad (\text{S27})$$

$$t'_{\uparrow 2} = t \sin(\lambda) \cos(\beta) e^{i\delta}, \quad (\text{S28})$$

$$t'_{\downarrow 2} = t \sin(\lambda) \sin(\beta) e^{i\delta}. \quad (\text{S29})$$

Omitting the prime from all quantities, we obtain the expressions stated in the main paper.

### Extraction procedure for toy model parameters from solutions for the 2D model

We next explain how we extract the parameters of the toy model from the eigenenergies and eigenstates of the 2D model, which are found numerically.

The first step is to consider only the two modes closest to zero energy and neglect all other modes:

$$H_{2D} \approx \frac{1}{2} \sum_{|l| \leq 2} \varepsilon_n \beta_l^\dagger \beta_l = \frac{1}{2} \boldsymbol{\beta}^\dagger \cdot \mathcal{H}'_I \cdot \boldsymbol{\beta}, \quad (\text{S30})$$

with  $\mathcal{H}'_I = \text{diag}(\varepsilon_1, \varepsilon_2, -\varepsilon_1, -\varepsilon_2)$ . Matching the eigenenergies (S4) for the toy model to those obtained from the 2D model fixes the parameters  $\Omega$  and  $\varepsilon$  to

$$\Omega = (\varepsilon_2 - \varepsilon_1)/2, \quad (\text{S31})$$

$$\varepsilon = \sqrt{\varepsilon_1 \varepsilon_2}. \quad (\text{S32})$$

To obtain the tunnel amplitudes for the toy model, we rotate the modes  $\beta_l$  such that the matrix representation of  $H_{2D}$  is given by Eq. (S3). This yields new modes  $\tilde{\alpha}_n$  whose wave function components yield the tunnel couplings as described in Sec. .

Clearly, one unitary transformation that transforms Eq. (S30) on the desired form is given by  $\tilde{\boldsymbol{\alpha}} = U^\dagger \boldsymbol{\beta}$ ; however, this is not the only possible transformation. The most general transformation includes an additional phase factor in the definition of the modes  $\beta_l$ , i.e.,  $\tilde{\boldsymbol{\alpha}} = U^\dagger \mathcal{W} \boldsymbol{\beta}$ , where  $\mathcal{W} = \text{diag}(e^{i\varphi_2}, e^{i\varphi_1}, e^{-i\varphi_1}, e^{-i\varphi_2})$ . The transformation  $\mathcal{W}$  leaves the form of Hamiltonian (S30) invariant. Note that the phase factors  $\varphi_1$  and  $\varphi_2$  correspond to phase choice for the eigenstates of  $\mathcal{H}_{\text{BdG}}$  and those can change randomly from one point to the next when applying a numerical diagonalization procedure.

The inclusion of the phase factors is important since it influences where the two modes

$$\tilde{\alpha}_l(\varphi_1, \varphi_2) = \sum_{\mathbf{n}, \sigma} [\tilde{u}_{l\mathbf{n}\sigma} \psi_{\mathbf{n}\sigma} + \tilde{v}_{l\mathbf{n}\sigma} \psi_{\mathbf{n}\sigma}^\dagger] \quad (\text{S33})$$

are localized within the stripe. Here, we use the components  $\tilde{u}_{l\mathbf{n}\sigma}$  and  $\tilde{v}_{l\mathbf{n}\sigma}$  of the solutions of the BdG equation in the tight-binding approximation, where  $\mathbf{n} = (n_x, n_y)$  denotes the lattice point ( $|n_x| \leq N_x/2, n_y \leq N_y/2$ ). Here,  $\psi_{\mathbf{n}\sigma}$  denotes the electron field operator with spin  $\sigma$  at lattice point  $\mathbf{n}$ . We next introduce a normalized 1D cut of the wave function along the symmetry axis of the stripe,  $\tilde{u}_{ln_y\sigma} = \tilde{u}_{ln_x=0n_y\sigma}/\sqrt{pl}$  and  $\tilde{v}_{ln_y\sigma} = \tilde{v}_{ln_x=0n_y\sigma}/\sqrt{pl}$  with  $pl = \sum_{n_y, \sigma} [|\tilde{u}_{ln_x=0n_y\sigma}|^2 + |\tilde{v}_{ln_x=0n_y\sigma}|^2]$ . For this 1D cut, we consider the probability to find a quasiparticle in mode  $l$  in the right half of the stripe:

$$P_l(\varphi_1, \varphi_2) = \sum_{n_y > 0, \sigma} [|\tilde{u}_{ln_y\sigma}|^2 + |\tilde{v}_{ln_y\sigma}|^2]. \quad (\text{S34})$$

It can be shown that  $P_2(\varphi_1, \varphi_2) = 1 - P_1(\varphi_1, \varphi_2)$ . Using a numerical optimization routine, we chose  $\varphi_1$  and  $\varphi_2$  such that  $P_1(\varphi_1, \varphi_2)$  is minimized. We emphasize that there is a freedom how to chose the phases  $\varphi_1$  and  $\varphi_2$  and this choice is therefore neither an approximation nor does it require any assumptions. For this specific choice of the phases, we identify  $\tilde{\alpha}_1(\varphi_1, \varphi_2) \equiv \alpha_L$  and  $\tilde{\alpha}_2(\varphi_1, \varphi_2) \equiv \alpha_R$ .

Up to this point, this procedure contains no other approximation than the restriction to the two lowest modes. In the toy model, we additionally neglect the tunnel couplings of mode  $\alpha_r$  to lead  $\bar{r}$ . This is why it is important

to use modes that are maximally localized at the two ends of the island. In this way, the toy model is a simplification as compared to a completely general model of a superconducting island with two modes. For the plots shown in the main paper, we find that the rotated modes with field operators  $\tilde{\alpha}_1, \tilde{\alpha}_2$  are well localized within one half of the stripe and therefore this approximation works very well.

## DETAILS OF THE CALCULATIONS

### Tight-binding calculations

For the numerical diagonalization of the Bogoliubov-de Gennes Hamiltonian (5), we use a tight-binding approach. The details are discussed in [2].

### Transport calculations

In this Section, we discuss the details of our transport calculations. We briefly describe our master-equation approach and the assumptions behind it. We further give important steps for the computation of the rates needed to set up the master equation and to compute the current.

In terms of the many-body basis  $|n, \boldsymbol{\eta}\rangle$  introduced in Sec. , the master equation takes the general form

$$\dot{P}_{\boldsymbol{\eta}} = - \left( \sum_{\boldsymbol{\eta}'} \Gamma_{\boldsymbol{\eta}'\boldsymbol{\eta}} \right) P_{\boldsymbol{\eta}} + \sum_{\boldsymbol{\eta}'} \Gamma_{\boldsymbol{\eta}\boldsymbol{\eta}'} P_{\boldsymbol{\eta}'}. \quad (\text{S35})$$

where  $P_{\boldsymbol{\eta}} = \langle n, \boldsymbol{\eta} | \rho_I | n, \boldsymbol{\eta} \rangle$  is the occupation probability of state  $|n, \boldsymbol{\eta}\rangle$  for the reduced density matrix  $\rho_I$  of the island. We do not take into account off-diagonal elements of the density matrix (coherences), which is a good approximation when  $\Gamma \ll |\varepsilon_{n, \boldsymbol{\eta}} - \varepsilon_{n, \boldsymbol{\eta}'}|$  for all states  $\boldsymbol{\eta}, \boldsymbol{\eta}'$  within each charge state. As mentioned in the main paper, we focus on the cotunneling regime, i.e., when only one charge state  $n = n_0$  is occupied. We take  $n_0$  to be even. Furthermore, we consider gate voltages where only states with charge  $n = n_0 + 1$  need to be included as virtual intermediate states, while the contribution from states with charge  $n = n_0 - 1$  may be neglected.

We solve for the stationary solution  $\dot{P}_{\boldsymbol{\eta}}^{\text{st}} = 0$  under the constraint  $\sum_{\boldsymbol{\eta}} P_{\boldsymbol{\eta}}^{\text{st}} = 1$  and compute the stationary current as

$$I^{\text{st}} = \sum_{\boldsymbol{\eta}'\boldsymbol{\eta}} (\Gamma_{\boldsymbol{\eta}'\boldsymbol{\eta}}^{RL} - \Gamma_{\boldsymbol{\eta}'\boldsymbol{\eta}}^{LR}) P_{\boldsymbol{\eta}}^{\text{st}}. \quad (\text{S36})$$

Here,  $\Gamma_{\boldsymbol{\eta}'\boldsymbol{\eta}}^{r'r}$  denotes a cotunneling process that transfers an electron from lead  $r$  to lead  $r'$ , where  $\Gamma_{\boldsymbol{\eta}'\boldsymbol{\eta}} = \sum_{r,r'} \Gamma_{\boldsymbol{\eta}'\boldsymbol{\eta}}^{r'r}$ .

In the case of the toy model, we restrict our calculations to two modes, which is a good approximation if

cotunneling through the quasiparticle continuum can be neglected. This requires the island to be long (quantization energy  $\pi^2/2m^*L^2 > \Delta$  provided the island is nearly depleted,  $\mu + E_{\text{SO}} \ll \Delta$ ) or the gap has to be large ( $\min(\varepsilon, \Omega), T, V_b \ll \Delta$ ).

The tunnel rates are obtained from the T-matrix approach [3],

$$\frac{\Gamma_{\boldsymbol{\eta}_f\boldsymbol{\eta}_i}}{2\pi} = \sum_{f,i} \rho_i \delta(E_f - E_i) |\langle \boldsymbol{\eta}_f, f | T(E_i) | \boldsymbol{\eta}_i, i \rangle|^2, \quad (\text{S37})$$

with the T-matrix

$$T(E) = H_T + H_T \frac{1}{E - H_I - H_0 + i0_+} H_T + \dots \quad (\text{S38})$$

In the above expression,  $\boldsymbol{\eta}_i$  ( $\boldsymbol{\eta}_f$ ) denotes the occupations of the island modes in the initial (final) state in charge state  $n = 0$ . Furthermore  $i$  ( $f$ ) refers to the initial (final) states of the lead, which we sum over, weighted by the probability  $\rho_i = e^{-\beta H_0} / \text{tr}(e^{-\beta H_0})$  for initial state  $i$  in the grand canonical ensemble. The many-body energies are given by  $E_{\alpha} = \omega_{\alpha} + \varepsilon_{n_0\boldsymbol{\eta}_{\alpha}}$ , where  $H_I |n_0, \boldsymbol{\eta}_{\alpha}\rangle = \varepsilon_{n_0\boldsymbol{\eta}_{\alpha}} |n_0, \boldsymbol{\eta}_{\alpha}\rangle$  (see Sec. ) and  $H_0 |\alpha\rangle = \omega_{\alpha} |\alpha\rangle$  for  $\alpha = i, f$ . The rates  $\Gamma_{\boldsymbol{\eta}'\boldsymbol{\eta}}^{r'r}$  ( $r' \neq r$ ) are obtained by accounting only for terms  $T(E) \sim H_T^r \frac{1}{\Delta E} H_T^{r'}$ , where  $H_T^r$  is the part of the tunnel Hamiltonian involving lead  $r$ .

We include in Eq. (S38) terms of  $O(t_D, t^2)$  and neglect higher-order terms, as well as terms of  $O(t, t_D^2)$  [even though they formally appear in the perturbation expansion of the T-matrix up to  $O(H_T^2)$ ]. The terms  $\sim t$  can be omitted because they correspond to sequential electron tunneling processes that are exponentially suppressed in the cotunneling regime. The effect of terms  $\sim t_D^2$  would be to add an additional contribution  $\delta I$  to the current. This corresponds to electron-pair tunneling through the reference arm, which does not exhibit a flux dependence as long as higher-order tunneling terms are neglected. An additional contribution  $\delta I$  would reduce the interference contrast in the MBS case somewhat but would not change the findings qualitatively. The contribution  $\delta I$  can, at least in principle, be made much smaller than the contributions we account for: Note that the largest interference contrast is given when  $t_D \sim t^2/U$ , i.e., when the conductances through the two arms are matched. This means that terms  $\sim t_D^2$  can be made smaller by scaling down  $t_D$  and  $t$  while keeping  $t_D \sim t^2/U$ .

Evaluating Eq. (S37), we get for the inelastic cotunneling rates

$$\frac{\Gamma_{\boldsymbol{\eta}_f\boldsymbol{\eta}_i}^{r'r}}{2\pi} = \sum_{rr'\sigma\sigma'\boldsymbol{\eta}\boldsymbol{\eta}'} \nu_r \nu_{r'} T_{r'\sigma'}^{\boldsymbol{\eta}\boldsymbol{\eta}_f*} T_{r\sigma}^{\boldsymbol{\eta}\boldsymbol{\eta}_i} T_{r'\sigma'}^{\boldsymbol{\eta}'\boldsymbol{\eta}_f} T_{r\sigma}^{\boldsymbol{\eta}'\boldsymbol{\eta}_i*} M(\varepsilon_{\boldsymbol{\eta}\boldsymbol{\eta}_i}^{10}, \varepsilon_{\boldsymbol{\eta}'\boldsymbol{\eta}_i}^{10}, \mu_r, \mu_{r'} + \varepsilon_{0\boldsymbol{\eta}_f} - \varepsilon_{0\boldsymbol{\eta}_i}), \quad (\text{S39})$$

and for the elastic cotunneling rates ( $\boldsymbol{\eta}_f = \boldsymbol{\eta}_i$ )

$$\begin{aligned} \frac{\Gamma_{\boldsymbol{\eta}_i \boldsymbol{\eta}_i}}{2\pi} &= \sum_{rr'} \nu_r \nu_{r'} \{2(1 + \tau_{\text{sf}}) |t_D|^2 K(\mu_r, \mu_{r'}) \\ &\quad - 2 \operatorname{Re} \sum_{\boldsymbol{\eta} \sigma \sigma'} t_D (\delta_{\sigma \sigma'} + \tau_{\text{sf}} \delta_{\sigma \bar{\sigma}'}) T_{r' \sigma'}^{\boldsymbol{\eta} \boldsymbol{\eta}_i *} T_{r \sigma}^{\boldsymbol{\eta} \boldsymbol{\eta}_i} \\ &\quad e^{i\pi \Phi / \Phi_0} L(\varepsilon_{\boldsymbol{\eta}_i}^{10}, \mu_r, \mu_{r'}) \\ &\quad + \sum_{\boldsymbol{\eta} \boldsymbol{\eta}' \sigma \sigma'} T_{r' \sigma'}^{\boldsymbol{\eta}' \boldsymbol{\eta}_i *} T_{r \sigma}^{\boldsymbol{\eta}' \boldsymbol{\eta}_i} T_{r' \sigma'}^{\boldsymbol{\eta} \boldsymbol{\eta}_i} T_{r \sigma}^{\boldsymbol{\eta} \boldsymbol{\eta}_i *} \\ &\quad M(\varepsilon_{\boldsymbol{\eta}' \boldsymbol{\eta}_i}^{10}, \varepsilon_{\boldsymbol{\eta} \boldsymbol{\eta}_i}^{10}, \mu_r, \mu_{r'})\}, \end{aligned} \quad (\text{S40})$$

with

$$K(\mu_r, \mu_{r'}) = \int d\omega f_r(\omega) (1 - f_{r'}(\omega)) \quad (\text{S41})$$

$$= (\mu_{r'} - \mu_r) b(\mu_{r'} - \mu_r), \quad (\text{S42})$$

$$L(E, \mu_r, \mu_{r'}) = \int d\omega \frac{f_r(\omega) (1 - f_{r'}(\omega))}{\omega - E + i0_+}, \quad (\text{S43})$$

$$M(E_1, E_2, \mu_r, \mu_{r'}) = \int d\omega \frac{f_r(\omega) (1 - f_{r'}(\omega))}{(\omega - E_1 + i0_+) (\omega - E_2 - i0_+)}. \quad (\text{S44})$$

with Fermi function  $f_r(\omega) = 1/(e^{(\omega - \mu_r)/T} + 1)$  and the Bose function  $b(\omega) = 1/(e^{\omega/T} - 1)$ .

To simplify the calculation of the integrals (S43) and (S44), we set  $\omega = 0$  in the denominators. This is a good approximation when temperature and voltage bias are small compared to energy differences between the island states in different charge sectors ( $T, V_b \ll U$ ). We obtain the approximate expressions

$$L(E, \mu_r, \mu_{r'}) \approx \frac{K(\mu_r, \mu_{r'})}{E}, \quad (\text{S45})$$

$$M(E_1, E_2, \mu_r, \mu_{r'}) \approx \frac{K(\mu_r, \mu_{r'})}{E_1 E_2}. \quad (\text{S46})$$

### Analytic expression for interference contrast

We next derive an analytic expression for the maximal interference contrast for the toy model in the case  $\beta = \delta = 0$ . We consider here the case of general bias voltage  $V_b$  and obtain the result (4) given in the main paper in the limit  $V_b \rightarrow 0$ .

For the toy model, the master equation takes the simple form

$$\begin{pmatrix} \dot{P}_+ \\ \dot{P}_- \end{pmatrix} = \begin{pmatrix} -\Gamma_{-+} & \Gamma_{+-} \\ \Gamma_{-+} & -\Gamma_{+-} \end{pmatrix} \begin{pmatrix} P_+ \\ P_- \end{pmatrix}, \quad (\text{S47})$$

where  $P_\eta$  denotes the occupation probability of state  $|n = n_0, \eta_1 = \eta_2 = (1 + \eta)/2\rangle$ . Note that there are only two

states denoted by  $\eta = \pm$  for each charge state because of the fermion-parity constraint  $(-1)^{\eta_1 + \eta_2} = (-1)^{n_0}$ . The stationary solution is simply given by

$$P_\pm^{\text{st}} = \frac{\Gamma_{\pm\mp}}{\Gamma_{+-} + \Gamma_{-+}}. \quad (\text{S48})$$

Assuming deep Coulomb blockade, i.e.,  $\varepsilon, \Omega \ll U$ , we approximate  $E_1 \approx E_2 \approx U$  in Eqs. (S45) and (S46) and obtain

$$\Gamma_{\boldsymbol{\eta}_f \boldsymbol{\eta}_i}^{r'r} = K_{\boldsymbol{\eta}_f \boldsymbol{\eta}_i}^{r'r} \frac{\gamma^2}{2} D_{\boldsymbol{\eta}_f \boldsymbol{\eta}_i}^{rr'} \quad (\text{S49})$$

$$\begin{aligned} \Gamma_{\boldsymbol{\eta}_i \boldsymbol{\eta}_i}^{r'r} &= K_{\boldsymbol{\eta}_i \boldsymbol{\eta}_i}^{r'r} \left\{ (1 + |\tau_{\text{sf}}|^2) \gamma_D + \frac{\gamma^2}{2} D_{\boldsymbol{\eta}_i \boldsymbol{\eta}_i}^{rr'} \right. \\ &\quad \left. - \sqrt{\gamma_D} \gamma \operatorname{Re}(e^{-i\pi \Phi / \Phi_0} C_{\boldsymbol{\eta}_i \boldsymbol{\eta}_i}^{rr'}) \right\} \end{aligned} \quad (\text{S50})$$

with  $\gamma_D = 2\pi |t_D|^2 \nu_L \nu_R$ ,  $\gamma_r = 2\pi |t_r|^2 \nu_r / U$ ,  $\gamma = \sqrt{\gamma_L \gamma_R}$ , and

$$K_{\boldsymbol{\eta}_f \boldsymbol{\eta}_i}^{r'r} = \frac{1}{\pi} K(\mu_r, \mu_{r'} + \varepsilon_{\boldsymbol{\eta}_f \boldsymbol{\eta}_i}), \quad (\text{S51})$$

$$C_{\boldsymbol{\eta}_f \boldsymbol{\eta}_i}^{r'r} = \frac{1}{t_r t_{r'}} \sum_{\boldsymbol{\eta} \sigma \sigma'} (\delta_{\sigma \sigma'} + \tau_{\text{sf}} \delta_{\sigma \bar{\sigma}'}) T_{r' \sigma'}^{\boldsymbol{\eta}_f \boldsymbol{\eta}_i *} T_{r \sigma}^{\boldsymbol{\eta}_f \boldsymbol{\eta}_i}, \quad (\text{S52})$$

$$D_{\boldsymbol{\eta}_f \boldsymbol{\eta}_i}^{rr'} = \frac{1}{t_r^2 t_{r'}^2} \sum_{\boldsymbol{\eta}' \boldsymbol{\eta} \sigma \sigma'} T_{r' \sigma'}^{\boldsymbol{\eta}' \boldsymbol{\eta}_f *} T_{r \sigma}^{\boldsymbol{\eta}' \boldsymbol{\eta}_f} T_{r' \sigma'}^{\boldsymbol{\eta} \boldsymbol{\eta}_i} T_{r \sigma}^{\boldsymbol{\eta} \boldsymbol{\eta}_i *}. \quad (\text{S53})$$

So far, no approximations regarding the tunnel couplings have been made.

We now limit our considerations to the case  $\beta = \delta = 0$ . By computing the above sums over the tunnel matrix elements, it is straightforward to show that  $D_{\boldsymbol{\eta}_f \boldsymbol{\eta}_i}^{r'r} = |C_{\boldsymbol{\eta}_f \boldsymbol{\eta}_i}^{r'r}|^2$ ,  $C_{\boldsymbol{\eta} \boldsymbol{\eta}}^{r'r} = 1$ ,  $C_{\boldsymbol{\eta} \boldsymbol{\eta}}^{rr} = 0$ ,  $C_{\boldsymbol{\eta} \boldsymbol{\eta}}^{\bar{r}r} = \cos(\rho) e^{i\eta\pi/2}$  and  $|C_{\boldsymbol{\eta} \boldsymbol{\eta}}^{\bar{r}r}| = \sin(\rho)$  with

$$\cos(\rho) = \frac{\cos(2\lambda)}{\sqrt{(\varepsilon/\Omega)^2 + 1}}. \quad (\text{S54})$$

Inserting the resulting expressions for the rates (S37) into the expression (S48) for the stationary occupations yields

$$P_\eta^{\text{st}} = \frac{G_\eta}{\sum_{\eta'} G_{\eta'}}, \quad (\text{S55})$$

and the stationary current reads for  $\tau_{\text{sf}} = 1$

$$\begin{aligned} \frac{I_{\text{st}}}{V_b} &= 2\gamma_D + \frac{\gamma^2}{2} \left[ \cos^2(\rho) + \sin^2(\rho) \sum_{\boldsymbol{\eta}} F_{\boldsymbol{\eta}} P_{\boldsymbol{\eta}}^{\text{st}} \right] \\ &\quad - \sqrt{\gamma_D} \gamma \cos(\rho) \sin\left(\pi \frac{\Phi}{\Phi_0}\right) (P_+^{\text{st}} - P_-^{\text{st}}), \end{aligned} \quad (\text{S56})$$

with

$$F_\eta = \sum_p (-1 + 2p\eta E/V_b) b(-pV_b + 2\eta E), \quad (\text{S57})$$

$$G_\eta = \sum_p (-p + 2\eta E/V_b) b(-pV_b + 2\eta E), \quad (\text{S58})$$

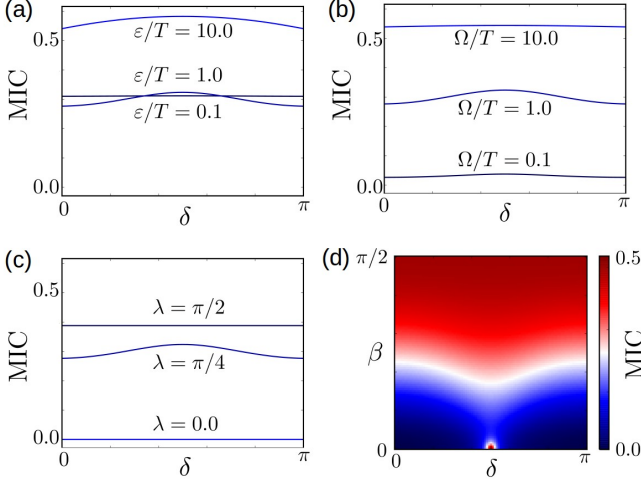


FIG. S1: Dependence of the MIC on the spin phase  $\delta$  of the Majorana couplings. Except for the parameters varied in each panel as indicated, we use the following parameters:  $\Omega/T = \varepsilon/T = 1$ ,  $\lambda = \beta = \pi/4$ ,  $V_b = 0.01T$ ,  $\delta = 0$ ,  $U = 100T$ .

where  $E = \sqrt{\Omega^2 + \varepsilon^2}$ . Finally, the maximal interference contrast reads

$$\text{MIC} = \frac{P_-^{\text{st}} - P_+^{\text{st}}}{2\sqrt{1 + \left(\frac{\varepsilon/\Omega}{\cos^2(2\lambda)} - 1\right) \sum_{\eta} F_{\eta} P_{\eta}^{\text{st}}}}. \quad (\text{S59})$$

In the limit  $V_b \rightarrow 0$ , one obtains

$$P_{\eta}^{\text{st}}(V_b = 0) = \frac{2e^{-\eta E/T}}{\cosh(E/T)}, \quad (\text{S60})$$

$$F_{\eta}(V_b = 0) = \frac{(\eta 2E/T - 1) + e^{-\eta 2E/T}}{2 \sinh^2(E/T)}, \quad (\text{S61})$$

and inserting this into Eq. (S59) yields Eq. (4) in the main paper.

## DISCUSSION OF RESULTS

### Toy model: Pathological case

As mentioned in the main paper, the case  $\Omega = 0$  combined with  $\lambda = 0$  or  $\varepsilon = 0$  is a pathological case of our model. The reason is that the mode  $\langle 23 \rangle$  decouples from the leads. The occupation probability of mode  $\langle 23 \rangle$  is then not determined by transport but by other parity-switching mechanisms not included in our model (e. g. quasiparticle poisoning). If this switching mechanism is much slower than the time window over which the current is averaged, one may measure a nonzero MIC. In this case, the parity of mode  $\langle 23 \rangle$  is fixed during that time and only parity-conserving tunnel processes happen. The interference patterns are then shifted by  $\pi$  with respect to each other depending on the parity of mode  $\langle 23 \rangle$ . This

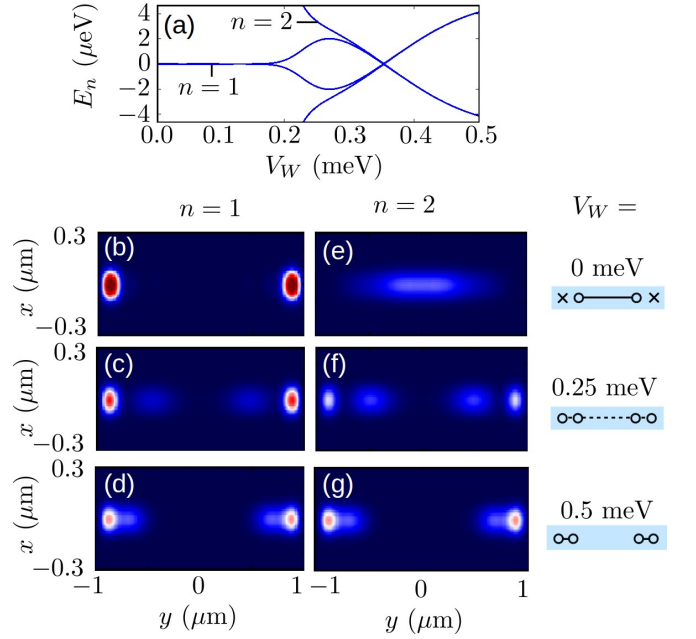


FIG. S2: Tuning the probability density of the eigenmodes with the wire potential. In (a), we show the same close-up as in Fig. 3(b) of the main paper. In (b) – (g), we show the probability density  $P(n_x, n_y) = \sum_{\sigma} [|u_{\sigma}(n_x, n_y)|^2 + |v_{\sigma}(n_x, n_y)|^2]$  of the lowest eigenmode ( $n = 1$ , left panels) and the next-to-lowest eigenmode ( $n = 2$ , right panels). The wire potential is varied as indicated to the right of the panels with the pictograms sketching the corresponding couplings of the Majoranas as in the toy model. Parameters are as in Fig. 3, left panel.

can be used to read out the parity of this mode as proposed earlier for Majorana box qubits [4]. Furthermore, each time a transition between ground and excited state happens, the current would switch in experiments (for fixed flux  $\Phi$ ). If the parity switching is instead fast compared to the current averaging time, the measurement will average over both patterns and the MIC is zero. The same reasoning also applies when  $\Omega/\varepsilon \rightarrow \infty$  and parity-flipping cotunneling processes are strongly suppressed.

### Toy model: Dependence of the maximal interference contrast on $\delta$

In Fig. S1, we show that the dependence of the interference contrast on  $\delta$  is very weak. The only exception is a spot close to  $(\beta = 0, \delta = \pi/2)$  [Fig. S1(d)].

### 2D island model: Tuning from two MBSs to two ABSs

In this Section, we discuss how the probability densities of the eigenmodes evolve when increasing the wire potential barrier  $V_W$  [Fig. S2]. For  $V_W = 0$ , there is one

mode ( $n = 1$ ) close to zero energy [Fig. S2(a)]. This mode is formed by slightly overlapping MBSs at opposite ends of the stripe [Fig. S2(b)]. The second mode ( $n = 2$ ) is at a large energy ( $\approx 0.6\Delta$ ) with a probability density delocalized along the stripe [Fig. S2(e)]. When increasing  $V_W$ , this mode comes close to and sticks to zero energy [Fig. S2(a)]. Its probability density is increasingly pushed to the end of the wire [Fig. S2(f)]. For large  $V_W$ , the two modes become nearly degenerate [Fig. S2(a)] and their probability densities become similar [Fig. S2(d) and (g)]. Here, the eigenstates are symmetric and antisymmetric combinations of slightly overlapping localized terminal ABSs, so that the probability densities have

equal weights on both ends.

---

- [1] E. Prada, R. Aguado, and P. San-Jose, Phys. Rev. B **96**, 085418 (2017).
- [2] M. Hell, K. Flensberg, and M. Leijnse, Phys. Rev. B **96**, 035444 (2017).
- [3] H. Bruus and K. Flensberg, *Many-body quantum theory in condensed matter physics: an introduction* (Oxford University Press, 2004).
- [4] S. Plugge, A. Rasmussen, A. Egger, and K. Flensberg, New Journal of Physics **19**, 012001 (2017).